Failure Analysis of S55C Medium Carbon Steel for the Pickup Crankshaft

Bundit Inseemeesak [1] and Visanu Boonmag [2,*]

[1] Automotive Manufacturing Engineering, Faculty of Engineering and Technology, Panyapiwat Institute of Management, Bangkok, Thailand
[2] Department of Mechanical Engineering, Faculty of Engineering, Thonburi University, Bangkok, Thailand
Email: banditins@pim.ac.th (B.I.); visanu396@yahoo.com (V.B.)
*Corresponding author

***Abstract*—There have been reports from service centers of important problems of a diesel engine crankshaft in mini trucks. All crankshafts crack from the same region, the fracture occurred in the first crankpin of the crankshaft. The crankshaft is made from JIS-S55C hardened medium carbon steel. A series of experiments including chemical analysis, macro and microstructural analysis, mechanical properties test, and numerical stress analysis. The results of fracture surface of this crankshaft were cause by fatigue with the detection of beach marks, ratchet marks, river marks, cleavage fracture and fatigue striations which these results indicate that the fracture mode of brittle fracture. The microstructure is composed of perlite-ferrite on the outer surface showed some coating nitriding layers, most hard coating is not found, the hardness test revealed an uneven hardness distribution, the maximum hardness on the center of the shaft measuring 309 HV, which is more than compared to the outer surface is 259 HV for these applications. It was found that the hardness value was abnormal. This is consistent with the experimental results of the surface microstructure which showed some coating layers, while the hard coating is not found. Besides, the numerical results also revealed that the first crankpin fillet was the most vulnerable to breakage, which is consistent with the mechanical experimental results. Finally, the summary analysis results are consistent with the hypothesis of this research and as an information for a prevent such failures crankshaft in the future.**

***Keywords*—pickup trucks, first crankpin, fatigue, nitriding layers, numerical stress analysis**

I. Introduction

The crankshaft is an important part in an engine, which converts the vertical motion of the piston into rotational motion. Because the crankshaft must be rotated throughout the life of the engine. Therefore, in the design process, fatigue performance and ductility are the main considerations. The crankshaft is used to support cyclic loads. Therefore, the crankshaft must be strong and durable for the long-term use of the vehicle. The crankshaft in an engine is often designed for infinite service life, but in operation there are many factors that can lead to the common types of crankshaft damage during use, such as the dimensions of the crankshaft, the crankshaft material, insufficient lubrication, torque, speed, stress, fatigue of the material, and behavior of the driver, etc. Fatigue is one of the most common events that occur under normal operation where alternating stresses are lower than destructive stresses. Fatigue failure usually begins at a critical area, whereby structural defects in materials and manufacturing processes cause the service life of the crankshaft to be primarily determined from this critical area [1].

Considering the literature review about failure analysis of crankshaft, Farrhi *et al.* [2] presented the failure analysis of the crankshaft in a four-cylinder diesel engine. FEM results revealed that the first crankpin fillet is the most vulnerable point to fracture and SEM images of the fractured surface also showed cleavage fracture put in evidence that the failure was brittle fracture. Optimization of the fillet rolling process by changing process parameters has been recommended to the manufacturer. Witek *et al.* [3] performed the failure analysis of the crankshaft of a diesel engine. The main reason for premature fatigue failure was high-cycle fatigue of the material in the external zone of the crank pin where the small structural radius was designed. A decrease of hardness is often related to decrease of yield stress and UTS of material. This phenomenon has an influence on limited fatigue life of the shaft material in the critical zone [3]. Khameneh *et al.* [4] examined high-cycle bending fatigue and fracture behaviors of the EN-GJS700-2 ductile cast iron. The main reason for the fracture surface of engine crankshafts is debonding of nodular graphites from the ferritic-pearlitic matrix, micro-cracks, the secondary crack, cleavage marks, scratching marks and inclusions [4]. Aliakbari *et al.* [5] examined the analysis of crankshaft failure in wheel loader diesel engine. The main reason for the fatigue cracks appeared on the surface of the crankpin might be created by the existence of oil impurities, the impurities on the surface of the crankpin, inappropriate machining on the surface of the crankpin or severe wear and pitting from insufficient lubricating. Mateus *et al.* [6] investigated the failure analysis of crankshaft in a 1.9 turbo diesel engine. The main reason for the crankshaft failure resulted from a

Manuscript received June 2, 2023; revised August 2, 2023; accepted August 31, 2023; published February 24, 2024.

fatigue process governed by normal stresses raised by two possible processes, namely, a notch in the crack initiation spot, or the crankshaft misalignment. Fonte *et al.* [7] investigated the failure analysis of diesel motor crankshaft. The root cause to be an inadequate tightening of the main bearing cap bolts revealed by fretting wear vestiges, and a high stress concentration on the outer side of the cap due to irregular geometry close to the cap top holes. Jiao *et al.* [8] presented the fracture failure analysis of KL crankshaft. The main reason factor of crankshaft failure is fatigue caused by overloading. Wang *et al.* [9] investigated the cause of crankshaft fracture in a mining high-pressure water pump. The main reason was fatigue fracture is dominant failure mechanism, with evidence of striation and beach marks, and multiple fatigue cracks. Fillet radius was a main factor for fatigue crack initiation, fatigue crack mostly located in the thread root of radial oil-hole. Aliakbari *et al.* [10] presented the failure cause of crankshaft in a four-cylinder light-duty truck diesel engine. The main reason for the crankshaft nodularity is about 70%, which crankshaft structures are usually acceptable greater than 80% of nodularity. Besides, the crankshaft crankpin had no hardened surface layer in the crankpin was caused by the growth of fatigue cracks in the fillet zone due to the cyclic force resulting from the combustion chamber pressure. Miranda *et al.* [11] investigated the cause of shaft failure in a speed reduction box. The fractography revealed the presence of beach marks and crack nucleation on the fracture surface. Besides, the Scanning Electron Microscopy (SEM) analysis found ratchet marks, secondary cracks, and fatigue striations. All this evidence confirmed that the shaft was fractured by fatigue. The material presented a huge number of inclusions present in the metallic matrix of the fracture surface.

The factors mentioned above are often observed from past research. Fatigue is one of the most common events occurring under normal operation. This research aims at identifying the causes of the failure of the crankshaft in a pickup truck. All crankshafts failed from the same region; the multiple crack origin of the fracture occurs at the first crankpin of the crankshaft. Several methods have been considered in analyzing this crankshaft failure, the geometric dimensions are measured with a high-precision instrument, the visually inspect to get an overview of the fracture, spectrophotometers are used to determine the chemical analysis of materials, hardness test and tensile testing to verify mechanical properties, then an Optical Microscopy (OM) and Scanning Electron Microscopy (SEM), the final step a numerical simulation is performed to analyze the stress of the crankshaft by the calculated bending moments and torsional moments.

II. Experimental Procedure

Determining the cause of the failure will require several experiments with the failed crankshaft. The first step is to measure the geometric dimensions with a 3D coordinate measuring machine. The failed crankshaft had to be examined macroscopically to get the overall picture, with images of the general characteristics of the fracture surface captured on a digital camera (Nikon D80). The fracture surface was then subjected to more detailed microscopic examinations using scanning electron microscopy (JEOL: JSM-7800F prime). The specimen was cut from a crankshaft as shown in Fig. 1.

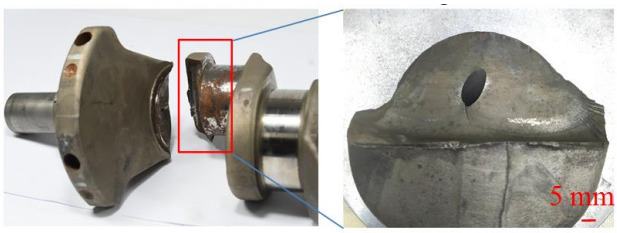

Fig. 1. Cutting position for macroscopic and microscopic examinations at 1x.

The second step carries out a material inspection to determine the chemical analysis and metallurgical structure with the requirements of the failed crankshaft material. The chemical analysis of the failed crankshaft material was determined using an optical emission spectrometer (Thermo: ARL 3,460). Metallographic examination of the failed crankshaft in a transverse cross-section was cold mounted using epoxy resin, then ground using emery paper (down to #1200 grit) and polished with 1-μm diamond paste. The microstructure was etched by using 2% nital solution (2 mL HNO_3 + 100 mL DI water) and microstructure was photographed using an optical microscope (Olympus laser microscopes: OLS 4,000).

Fig. 2. Tension testing equipment including (a) The tensile testing machine (b) The geometry of the standard specimen (all dimensions are in millimeter).

The third step, mechanical properties test, micro-hardness was measured using an ANTON PAAR: MHT-10 with a diamond indentation with a pyramidal angle of 136° and pressing load of 300 g to create a hardness profile from the shaft surface through the central axis and to align the indentation to the other surface, to one side of the crankshaft near the surface area of the fracture surface under ASTM E92-82 (Reapproved 2003). The tensile test is performed by SHIMADZU: EHF-EV101K2-070-0A and the specimens are cut with an EDM wire-cut machine into 2 pieces with a 6 mm diameter inner and 110 mm length from the failed crankshaft as shown in Fig. 2. In Fig. 3(a) shows the characteristics of the two specimens before the tensile test and Fig. 3(b) shows two specimens that have broken apart after the tensile test.

The fourth step, the numerical stress analysis, finite elements were performed using the ANSYS Workbench simulator. The software uses linear equations that govern the x, y and z axis motion behavior, parameters related to numerical simulation. ANSYS Workbench is software for analyzing bending moments and torsional moments in crankshaft structures. The geometry obtained from the Solid work program will be the initial one obtained from the crankshaft. After that, the finite element model is determined from the relevant parameters. The problem analysis and verification results are important factors that occur in the crankshaft under load that can be summarized for use in conjunction with the technical analysis obtained from the experiment.

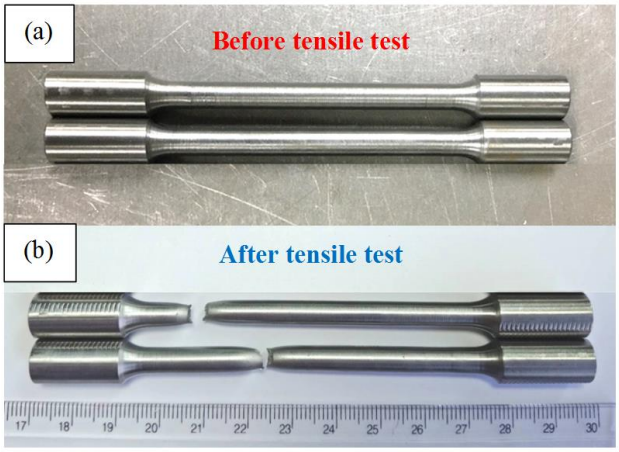

Fig. 3. The standard specimen including (a) Two specimens before tensile test. (b) Two specimens broken apart after the tensile test.

III. Results and Discussion

A. Fracture Surface Analysis

An analysis of the fracture surfaces of the crankshaft at low magnification by zoom stereo microscope is shown in Fig. 4 revealing where multiple crack origins actually started. The crack then expands slowly through the fatigue zone, an area that has been failed by cyclic loading. During this slow crack propagation, there is a change in load which corresponds to the crack growth rate that appears on beach marks.

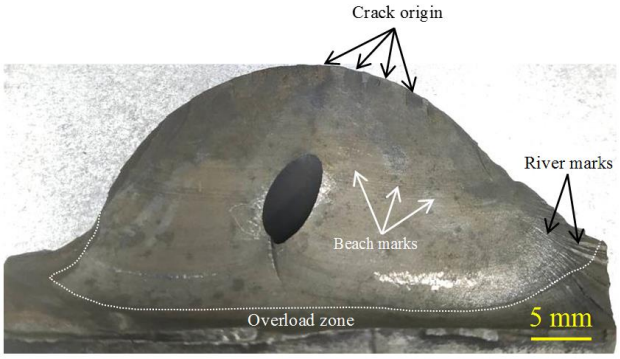

Fig. 4. Fracture characteristics of the crankshaft caused by fatigue.

In addition, there are two other important features that appear on the fracture surface from fatigue of the crankshaft. The first of these is the ratchet mark in Fig. 5 shows the boundary or line between two crack origins, and the ratchet mark is between them. The fracture images of the failed crankshaft, it was found that the fracture had multiple origins and because of the workpiece subjected to high total stress or the area is a stress concentration point. The second important feature is the shape of the fracture as a river mark as shown in Fig. 5, because the appearance on the fracture surface is like that of tributary rivers. The pattern predominantly shows the rapid expansion of the fatigue zone and shows the direction of crack propagation.

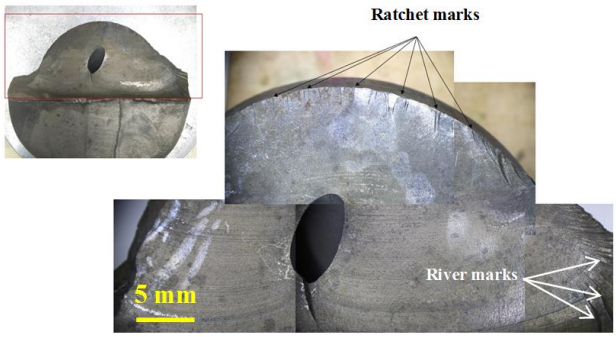

Fig. 5. Fracture images of the crankshaft shows ratchet marks and river marks at 1x.

Examine the fracture surface of the failed crankshaft by scanning electron microscopy. A photograph of the central region fracture is shown beach marks in Fig. 6(a). Fig. 6(b) High magnification images in the same area reveal a cleavage fracture near the central region of the fracture [12]. A photograph at the surface region using a scanning electron microscope shows the crankshaft fracture area in Fig. 7(a). Expansion of beach marks on most fractured surfaces are wavy lines that leave a mark on the beach, while Fig. 7(b) shows an enlarged section showing fatigue striations showing the direction of displacement between atoms, with fatigue striations in each stress period or each stress cycle acting on the specimen. These lines can only be seen by examination using a high-powered microscope [12]. Therefore, cleavage fracture is the fracture failure form of the crankshaft, and fatigue striations is the fatigue fracture feature.

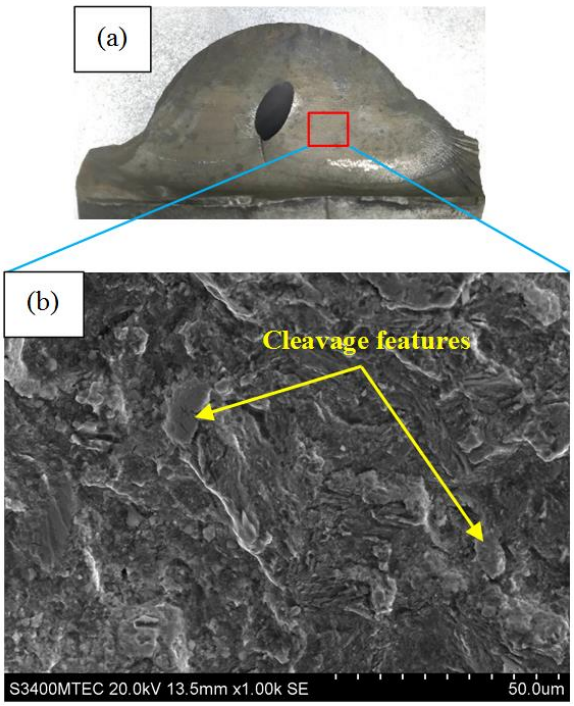

Fig. 6. SEM micrograph showing (a) Beach marks at 1x. (b) High magnification with cleavage fracture at 1.00kx, 50 µm.

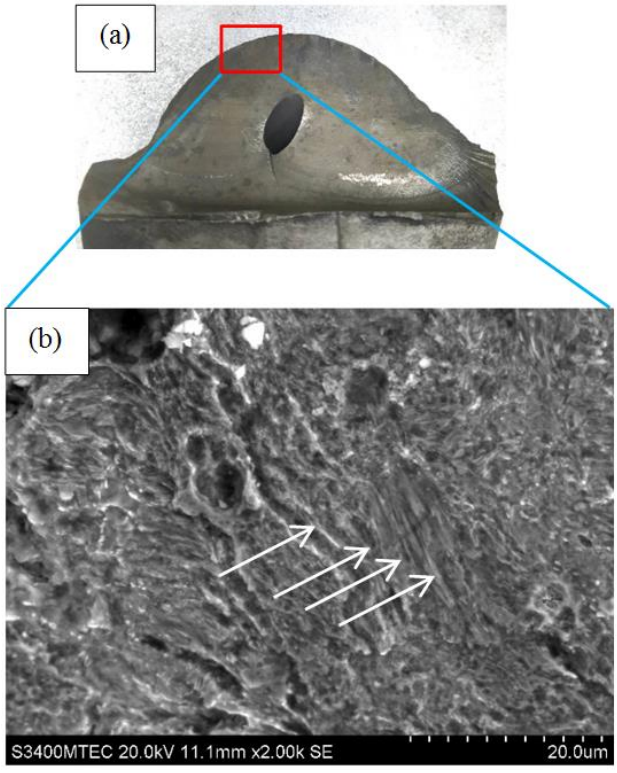

Fig. 7. SEM micrograph showing (a) SEM micrograph showing 1x. (b) Magnification of the visible fracture area showing fatigue striations and the direction of motion between dislocations of atoms at 2.00kx, 20 µm.

B. Material Inspection

The chemical analysis of the failed crankshaft material using a spectrophotometer test machine. The results of chemical analysis conducted on the failed crankshaft are presented in Table I. This analysis shows that the failed crankshaft is made of medium carbon steel and satisfies the technical requirements as per JIS G4051: Standard grade S55C [13].

TABLE I. CHEMICAL ANALYSIS OF THE FAILED CRANKSHAFT AND THOSE OF JIS-S55C STEEL (%wt)

Materials	Failed crankshaft	JIS-S55C [13]
C	0.568	0.52–0.58
Si	0.25	0.15–0.35
Mn	0.802	0.60–0.90
P	0.0178	≤0.030
S	0.0349	≤0.035
Cr	0.147	≤0.20
Mo	0.0076	≤0.30

Metallographic examinations as shown in Fig. 8(b) presents the same image at magnification 200 × 40 µm. In Fig. 8(c) the surface of the crankshaft shows that the microstructure is composed of perlite-ferrite with a hard coating layer or nitriding layer about 500 mm in size.

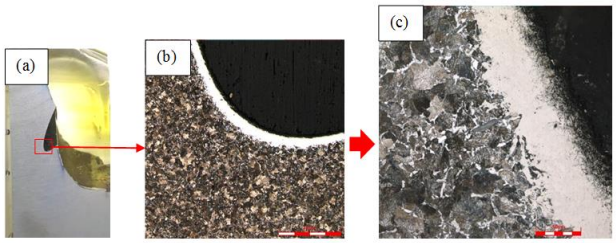

Fig. 8. Optical photomicrograph of the failed crankshaft. (a) Low magnification image of the failed crankshaft approximation 1x. (b) The same image at magnification 200×40 µm. (c) Magnification of the surface is composed of perlite-ferrite with a hard coating layer or nitriding layer about 500 micrometers in size with a magnification of 1000×50 µm.

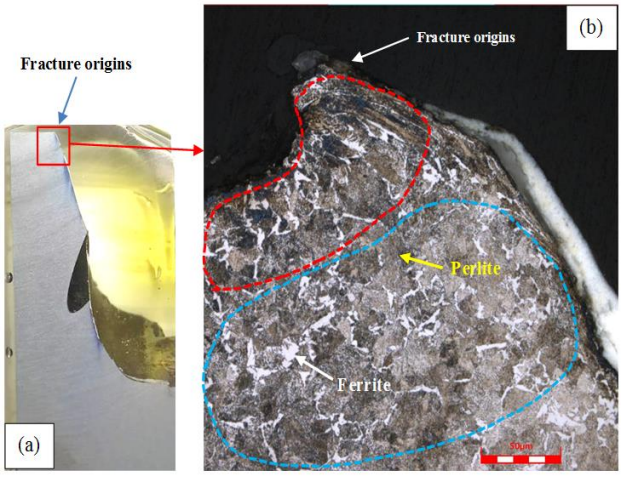

Fig. 9 Optical micrographs of failed crankshaft show (a) Low magnification image (1x) at the outer surface of the shaft. (b) shows the microstructures are perlite-ferrite grain boundary on the fracture initiation region at magnification 500×50 µm.

The fracture initiation region at the outer surface of the failed crankshaft is shown in Fig. 9(a), the fracture origins in an example. Fig. 9(b) is the same image at

magnification 500×50 µm at the fracture origin in the red line color, found that the ferrite (white) has a fine grain boundary, and in the blue line color on the fracture expansion zone, it was found that the ferrites had coarse grain boundary than those at the fracture initiation region. Therefore, the size of the grain boundaries of ferrite resulting in decrease mechanical properties and the strength of the material, also have the effect on the fatigue strength of these specific areas [11]. Fig. 10(a) shows low magnification image (1x) with two telescopes at the surface and core of the shaft. Fig. 10(b) The cross-section and microstructure of the outer surface showed some coating layers, most hard coating is not found. Fig. 10(c) The central axis of the crankshaft contains a perlite-ferrite microstructure and manganese sulfite inserted in the ground metal.

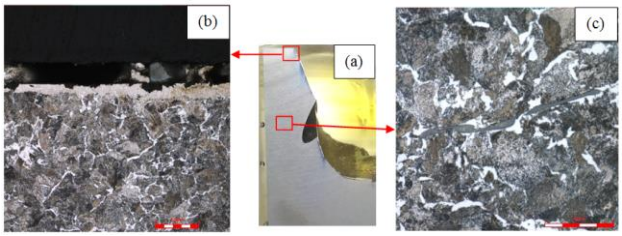

Fig. 10. Optical photomicrograph of the failed crankshaft. (a) Low magnification image of failed crankshaft approximation 1x. (b) Magnification of the outer surface composed of perlite-ferrite showed some coating layers, most hard coating is not found, magnification 500× 50 µm. (c) Magnification of the central axis is composed of perlite-ferrite and found manganese sulfite inserted in the ground metal, magnification of 1000×40 µm.

C. Mechanical Properties Test

In addition, the microhardness measurement of the cross-section is initiated by pressing from the outer surface of the crankshaft through the center axis in all 25 points of the crankshaft as shown in Fig. 11. The results of the hardness test are shown in Fig. 12, the maximum hardness on the center of the shaft measuring 309 HV, which is more than compared to the outer surface is 259 HV for these applications. It was found that the hardness value was abnormal. This is consistent with the experimental results of the surface microstructure which showed some coating layers, while the hard coating is not found.

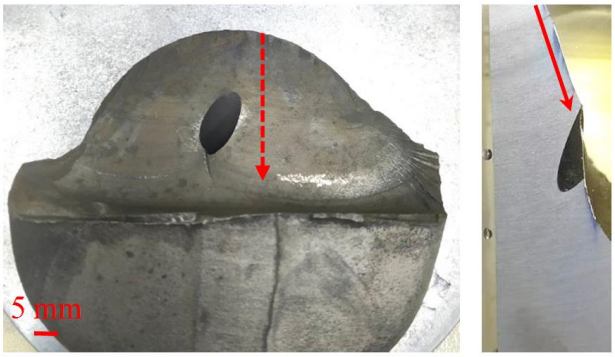

Fig. 11. The failed crankshaft hardness measurement line is measured from the case to the core of the shaft at 1x.

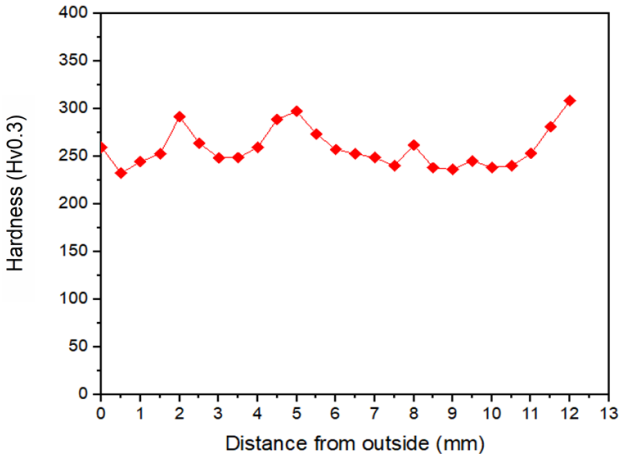

Fig. 12. The graph shows the hardness layer of the failed crankshaft.

TABLE II. TENSILE PROPERTIES TEST OF FAILED CRANKSHAFT

Materials	Ultimate tensile strength (MPa)	Yield strength (MPa)	Elongation (%)
Failed crankshaft 1	813.251	502.018	11.3075
Failed crankshaft 2	817.604	510.892	11.1219
JIS-S55C [13]	650–880	350–550	8–25

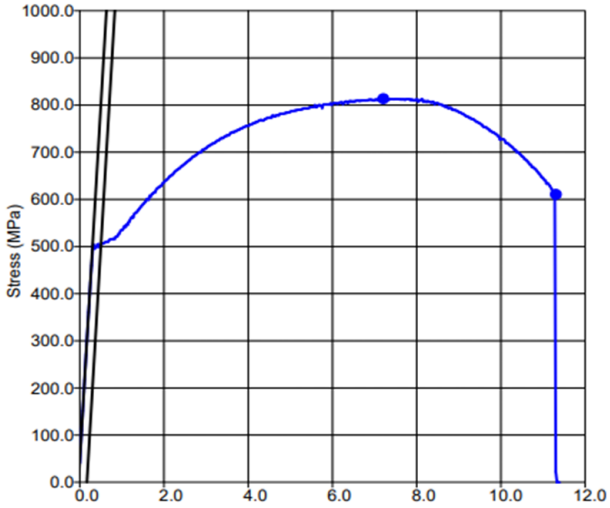

Fig. 13. Stress-strain curves of failed crankshaft material S55C steel at ambient temperature.

Mechanical properties of great importance are tensile tests, which this test will be ultimate tensile strength (S_{ut}), elongation and yield strength (S_y) and both properties of yield strength and ultimate tensile strength are criteria for resistance to deformation of a material and fracture, respectively. A tensile test was performed on two specimens obtained from the failed crankshaft of a pickup truck. The tensile properties of crankshaft materials compared to the S55C steel properties of standard materials are shown in Table II, and in Fig. 13 a stress-strain curve is illustrated. Observing the data from Table II showing the ultimate tensile strength and overall elongation of crankshaft materials within the tolerance

range of standard materials. However, the yield strength is about 9% lower than the high limit of standard material S55C steel [14].

D. Numerical Stress Analysis

There have been reports of diesel engine crankshaft damage in pickup trucks during operation. There were 10 broken crankshafts out of 500 pickup trucks in use. This data was obtained from a car service center in Thailand with a data collection period of 1 year. Details of diesel engine specifications are shown in Table III. Most of the information found in the report shows that many crankshafts fail prematurely.

TABLE III. ENGINE SPECIFICATIONS

Description	Values	Unit
Piston displacement	2499	cc
Bore x Stroke	95.4×87.4	mm
Compression ratio	18.1: 1	-
Maximum Power	100/3600	kW/rpm
Maximum Torque	320/2800	N-m/rpm
Maximum pressure	32	bar

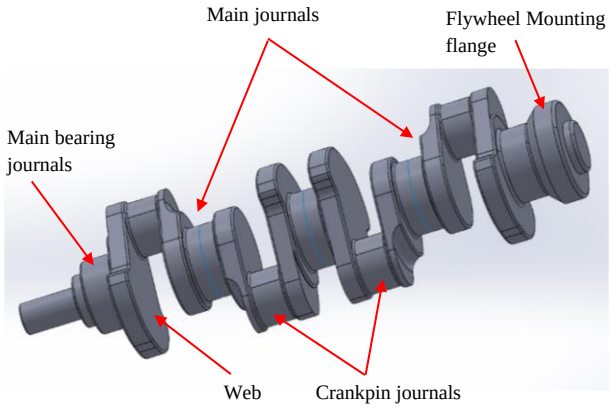

Fig. 14. 3D model of the crankshaft obtained from Solid works program.

Crankshaft dimensions and component names are as shown in Fig. 14. The parameters and dimensions of the crankshaft, such as the crankpin length and compression of the engine, can be used as parameters to determine the size of the crankshaft as shown in Table IV.

TABLE IV. DIMENSIONS OF THE CRANKSHAFT

Parameter	Value
Crankpin diameter	52 mm
Main shaft diameter	70 mm
Thickness of the crank web	20 mm
Length of the crankpin	155 mm
Young's modulus	200 GPa

To determine the stress distribution at the stress concentration of the crankshaft using the finite element method is very important and compared with the fracture initiation region. Determination of the actual stress for the stress concentration point. It is necessary to accurately assess the torsion acting on the structure of the crankshaft in diesel engines. The first step, the subsequent force and stress analysis paper, includes research related to the crankshaft mechanism of a reciprocating engine as shown in Fig. 15. The force acting on the piston and the subsequent stress on the crankshaft is the result of the maximum pressure P_{max} after combustion of the air-fuel mixture in the combustion chamber. When the crank angle φ changes, the piston force F_P acting on the crankpin of crankshaft which is generated by the force from the engine piston. As shown in Fig. 15 [15], this is the result of superposition of the oscillating inertial force F_{os} on the gas force F_G:

$$F_P = F_G + F_{os} \quad (1)$$

$$F_G = P_{\max} A_P \quad (2)$$

$$F_{os} = m_{os} a \quad (3)$$

The piston cross-section A_p, the oscillating mass m_{os}, the instantaneous acceleration of the piston a [15].

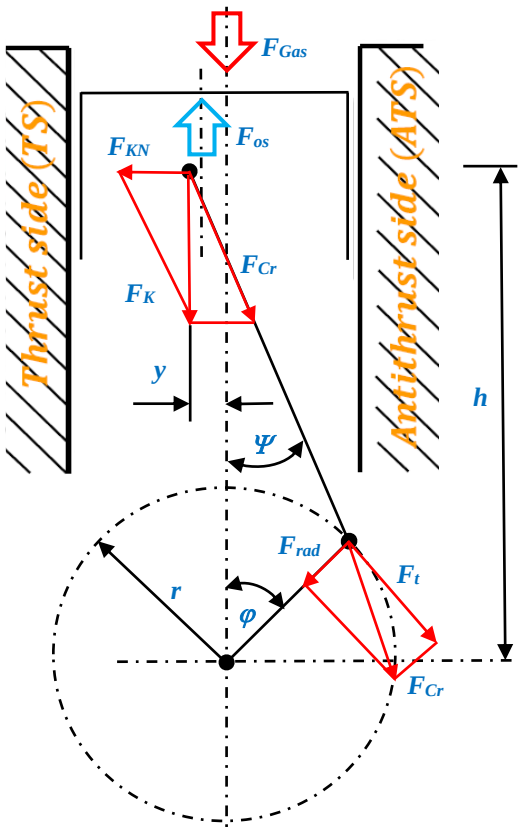

Fig. 15. The force acting on the piston in the engine, offset piston pin [15].

The inclination angle of the connecting rod with the axis line of the piston stroke ψ, the thrust in the connecting rod F_{cr} is achieved using dividing the force exerted on the piston F_P:

$$F_{cr} = \frac{F_P}{\cos\psi} \quad (4)$$

The tangential force exerted F_t and the radial force F_{rad} operate on the crankpin radially and subsequently as follows:

$$F_t = F_{cr}\sin(\psi+\varphi) \quad (5)$$

$$F_{rad} = F_{cr}\cos(\psi+\varphi) \quad (6)$$

The relationship between the angle of crank φ and the pivoting angle of the connecting rod ψ is as follows:

$$\Psi = \sin^{-1}(\sin\psi/\lambda) \quad (7)$$

where, $\lambda = l/r$ is the length ratio of the connecting rod to the crank radius (the quotient of the crank radius r and connecting rod length l).

The crank radius r as a lever arm and the distance between the crankpin bearing center to web-center b, the tangential force F_t and the radial force F_{rad} generate the torsional T and the bending moment M as follows:

$$T = F_t \times r \quad (8)$$

$$M = F_{rad} \times b \quad (9)$$

Therefore, the maximum bending σ_{max} and maximum shear stresses τ_{max}, load dynamic factor of bending moment Cm, and load dynamic factor of torsion Ct.

$$\sigma_{max} = \frac{16}{\pi d^3}(C_m M + \sqrt{(CmM)^2 + (C_t T)^2} \quad (10)$$

$$\tau_{max} = \frac{16}{\pi d^3}(\sqrt{(CmM)^2 + (C_t T)^2} \quad (11)$$

The next step is to stress field analysis. The crankshaft that can be generated from SolidWorks program is based on the actual failed crankshaft, after which it is stress analyzed by numerical simulation shown in Fig. 16 [14].

The final step was to determine the mechanical properties of the crankshaft material by entering a modulus of elasticity of 200,000 MPa, a density of 7.7 g/cm^3, and a Poisson's ratio of 0.3 [13], boundary conditions, loading and mesh type selection applied to this numerical simulation refer to [16]. Table II is used to apply mechanical and loading properties respectively. Axial load distribution towards the bearing of 120 degrees uniform pressure over the contact area. The load distribution was experimentally performed using the method of Webster *et al.* [17], and a numerical simulation method followed the method of Zhang *et al.* [18]. Elements of the Tetrahedral type were selected to the generated mesh operation models have 44,922 total elements, 76,410 total nodes and 43,655 Degrees of Freedom (DOF) for mesh control x, y, and z axes only, which is suitable for complex geometries. According to the engine's maximum pressure of 32 bar, the bore diameter and the maximum torsion values in Table III, the bending moment and torsion according to Fig. 16 are applied in the stress analysis on the crankshaft. The maximum equivalent von Mises stress in Fig. 17 at the crankpin-web zone of the crankshaft is 30.746 MPa, which is 6% of the yield strength of the crankshaft standard material S55C steel [15]. Consider Fig. 18 showing a minimum safety factor min is 2.80. It is evident in these cases that the result given by the calculation method and the finite element analysis are very similar.

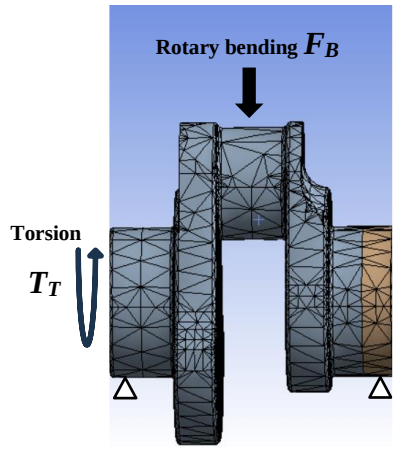

Fig. 16. Characteristics of the mesh control and the force acting on the crankpin of crankshaft.

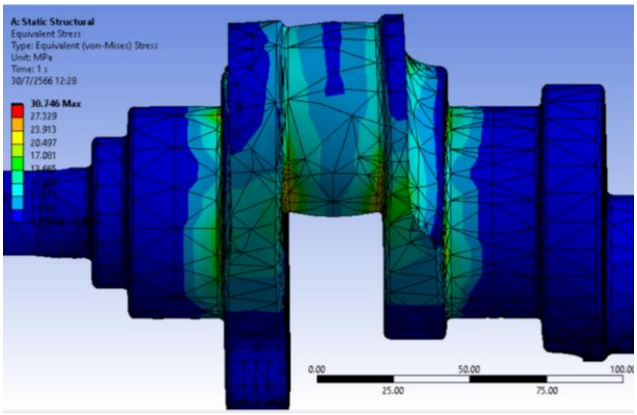

Fig. 17. The von Mises stress distribution in the web fillet of crankpin and fracture region.

Safety factor

$$n_f = \frac{S_e}{\sigma'_{max}} \quad (12)$$

σ'_{max} is midrange and alternating stress = 30.746 MPa

S_e is the endurance limit at the critical location of a machine part in the geometry and condition of use

$$S_e = k_a k_b k_c k_d k_e k_f S'_e \quad (13)$$

k_a is the surface condition modification factor = 1

k_b is the size modification factor.

$k_b = 1.51d^{-0.157} = 1.51 \times 104^{-0.157} = 0.73$ [19]

k_c is the load modification factor = 0.59 is the torsion.

k_d is the temperature modification factor = 1 [19].

k_e is the reliability factor.

$k_e = 1 - 0.08\, z_a = 1 - (0.08 \times 2.326) = 0.82$ [19].

k_f is the miscellaneous-effects modification factor.

k_f = 0.5 is nitriding hardened [19].

$S_e^{'}$ = rotary-beam test specimen endurance limit = $0.5 \times 880 = 440$ MPa

Substitute the parameter values in Eq. (13).

$$S_e = 1 \times 0.73 \times 0.59 \times 1 \times 0.82 \times 0.5 \times 440 = 77.70 \text{ MPa}$$

$$n_f = \frac{S_e}{\sigma_{\max}^{'}} = \frac{77.70}{30.746} = 2.52$$

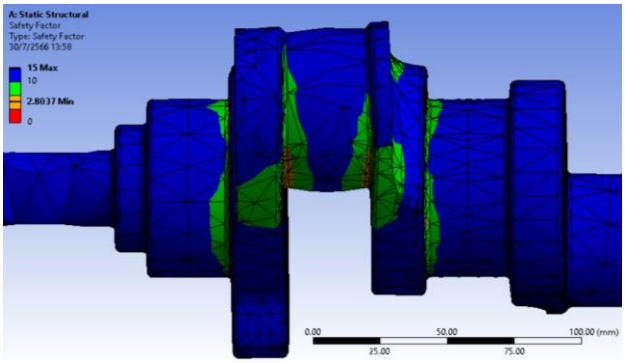

Fig. 18. The safety factor obtained from the numerical simulation.

Based on the results of numerical simulation using the ANSYS Workbench program as shown in Fig. 19, the maximum equivalent von Mises stresses in the crankshaft can be observed to deliver a maximum deformation at the junction between the first crankpin and the web, similar to the appearance of crankshaft cracks caused by fatigue after use for 125,000 km. In conclusion, the cause of the crankshaft damage is the fatigue of the shaft material.

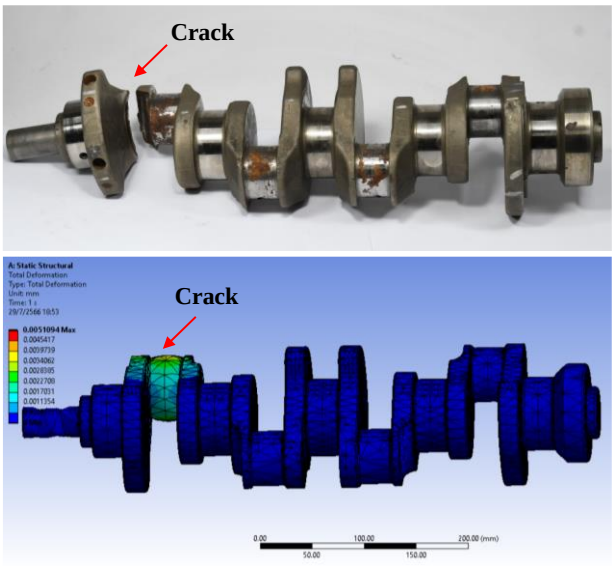

Fig. 19. Comparison of crack appearance between actual usage and stress obtained by simulation using ANSYS Workbench program.

IV. Conclusion

1. The morphological attributes of ratchet marks and river marks often give rise to stratified structures with diminished tear resistance. Elevated sulfide content, as evidenced by the morphologies of ratchet marks and river marks, emerges as a pivotal factor in facilitating the formation of crack initiation sites. Cleavage fracture delineates the predominant mode of failure in the crankshaft, whereas fatigue striations serve as discernible characteristics indicative of fatigue-induced fractures.
2. Chemical analysis reveals that the crankshaft is made of JIS-S55C steel. The microstructure is composed of perlite-ferrite on the outer surface showed some coating layers, most hard coating is not found.
3. The hardness test revealed an uneven hardness distribution, the maximum hardness on the center of the shaft measuring 309 HV, which is more than compared to the outer surface is 259 HV for these applications. It was found that the hardness value was abnormal. This is consistent with the experimental results of the surface microstructure which showed some coating layers, while the hard coating is not found.
4. The tensile test results of the 2 specimens obtained from the failed crankshaft material showed that the elongation and tensile strength values were within the standard values. However, the yield strength was below the high limit value of JIS-S55C standard steel material by about 9%.
5. Numerical simulation results showed the maximum equivalent von Mises stress at the crankpin-web zone of the crankshaft is 30.746 MPa, which is 6% of the yield strength of the crankshaft standard material S55C steel.
6. The results from the numerical simulation present the total deformation at the web crankpin fillet zone, which is similar to the appearance of crankshaft cracks caused by fatigue after the usage for 125,000 km. In conclusion, the cause of the crankshaft damage is the fatigue of the shaft material.

Conflict of Interest

The authors declare no conflict of interest.

Author Contributions

Visanu Boonmag contributed to this research by implementing the experimental and analytical work with the guidance and supervision from Bundit Inseemeesak. All authors had approved the final version.

Acknowledgment

This study was supported by Automotive Manufacturing Engineering, Faculty of Engineering and Technology, Panyapiwat Institute of Management for

research equipment and facilities. The authors would like to thank the National metal and materials technology center (MTEC) for their help and guidance during my research.

REFERENCES

[1] L. H. Zhao, Q. K. Xing, J. Y. Wang, S. L. Li, and S. L. Zheng, "Failure and root cause analysis of vehicle drive shaft," *Engineering Failure Analysis.* vol. 13, pp. 225–234, 2019.

[2] G. H. Farrahi, F. Hemmati, S. M. H-Gangaraj, M. Sakhaei, and S. Abolhassani, "Failure analysis of a four cylinder diesel engine crankshaft made from nodular cast iron," *The Journal of Engine Research*. vol. 18, pp. 21–27, 2010.

[3] L. Witeka, M. Sikorab, F. Stachowicza, and T. Trzepiecinskia, "Stress and failure analysis of the crankshaft of diesel engine," *Engineering Failure Analysis*. vol. 17, pp. 703–712, 2017.

[4] M. J. Khameneh and M. Azadi, "Evaluation of high-cycle bending fatigue and fracture behaviors in EN-GJS700-2 ductile cast iron of crankshafts," *Engineering Failure Analysis.* vol. 85, pp. 189–200, 2018.

[5] K. Aliakbari, N. Safarzadeh, and S. S. Mortazavi, "Analysis of the crankshaft failure of wheel loader diesel engine," *International Journal of Engineering*, vol. 31, pp. 473–479, 2018.

[6] J. Mateus, V. Anes, I. Galvão, and L. Reis, "Failure mode analysis of a 1.9 turbo diesel engine crankshaft," *Engineering Failure Analysis.* vol. 19, pp. 394–406, 2019.

[7] M. Fonte, M. Freitas, and L. Reis, "Failure analysis of a damaged diesel motor crankshaft," *Engineering Failure Analysis*, vol. 102, pp. 1–6, 2019.

[8] A. Jiao, B. H. Liu, X. M. Chen, X. B. Zou, and F. H. Wang, "Fracture failure analysis of KL crankshaft," *Engineering Failure Analysis*, vol. 20, 104498, 2021.

[9] H. Wang, S. Y. Yang, L. H. Hana, H. Fan, Q. F. Jiang, "Failure analysis of crankshaft of fracturing pump," *Engineering Failure Analysis*. vol. 109, 104378, 2020.

[10] K. Aliakbari, "Failure analysis of ductile iron crankshaft in four-cylinder diesel engine," *International Journal of Metal casting*. vol. 15, pp. 1223–1237, 2021.

[11] R. S. Miranda, C. Cruz, N. Cheung, and A. P. A. Cunha, "Fatigue failure analysis of a speed reduction shaft," *Metals*, vol. 11, 856, 2021.

[12] W. D. Callister, *Materials Science and Engineering an Introduction*, 7th ed. John Wiley & Sons, Inc, 2007, pp. 211–215.

[13] China steel suppliers. (2020). Data Table for: Steel Grades: Carbon Steel: S55C. [Online]. Available: https://www.steelgr.com/Steel-Grades/Carbon-Steel/s55c.html

[14] J. Langari, K. Aliakbari, R. M. Nejad, and S. K. Abbasnia, "Failure analysis of CK45 steel crankshaft in light truck diesel engine," *Engineering Failure Analysis*. vol. 145, 107045, 2023.

[15] K. Aliakbari, R. M. Nejad, T. A. Mamaghani, P. Pouryamout, and H. R. Asiabaraki, "Failure analysis of ductile iron crankshaft in compact pickup truck diesel engine," *Structures*, vol. 36, pp. 482–492, 2022.

[16] R. M. Nejad, K. Aliakbari, S. K. Abbasnia, and J. Langari, "Failure analysis of overdrive gear of passenger car gearbox fabricated from powder metallurgy," *Engineering Failure Analysis*. vol. 141, 106683, 2022.

[17] W. D. Webster, R. Coffell, and D. Alfaro, "A three dimensional finite element analysis of a high speed diesel engine connecting rod," *SAE Technical Paper*, 1983.

[18] G. Zhang, C. Wang, and G. Pu, "Fatigue life prediction of crankshaft repaired by twin arc spraying," *J. Cent. South Univ. Technol.,* vol. 12, pp. 70–76, 2005.

[19] J. E. Shigley, *Mechanical Engineering Design*, 9th ed. McGraw-Hill Book Company, 2008, pp. 733–775.